Title

II. A Study of Angle-resolved Photoemission Extended Fine Structure asApplied to the Cu 3s and Cu 3p Core-Levels of a Clean Cu(111) Surface

Author

Huff, W.R.A.

Publication Date

1996-02-26

LBL-38424
UC-401
Preprint

Lawrence Berkeley Laboratory
UNIVERSITY OF CALIFORNIA

Accelerator & Fusion
Research Division

Submitted to Physical Review B

II: A Study of Angle-Resolved Photoemission Extended Fine Structure as Applied to the Cu 3s and Cu 3*p* Core-Levels of a Clean Cu(111) Surface

W.R.A. Huff, Y. Chen, S.A. Kellar, E.J. Moler, Z. Hussain,
Y. Zheng, and D.A. Shirley

February 1996

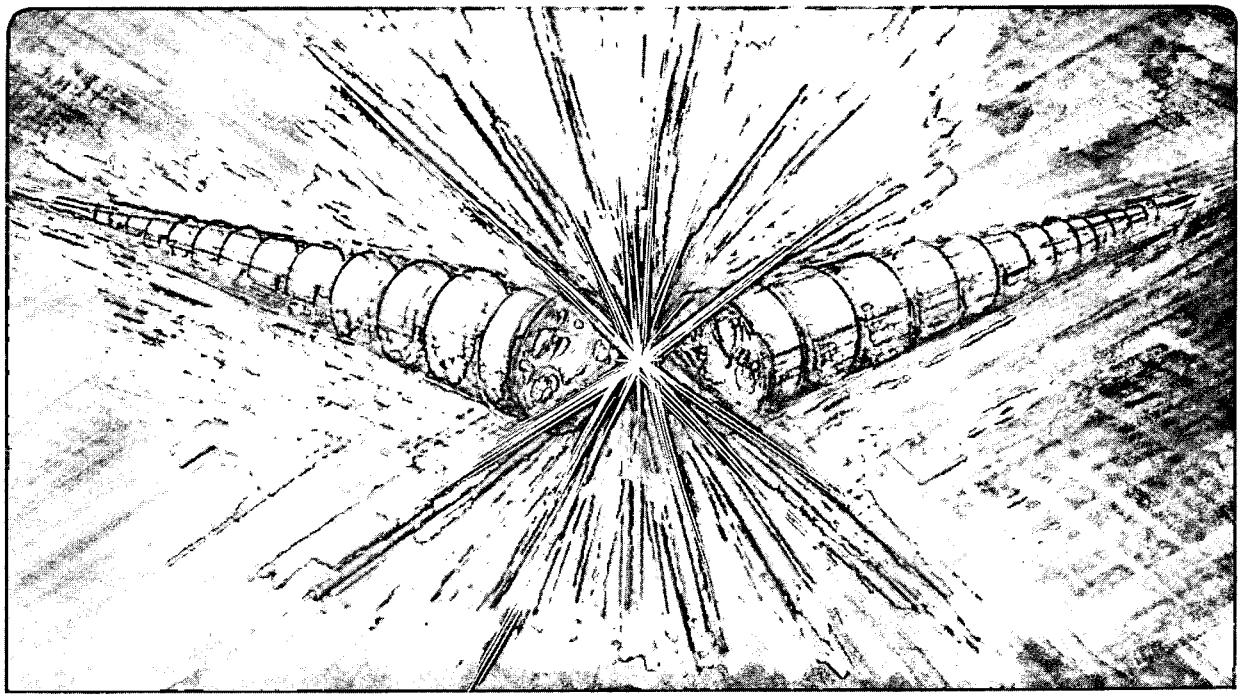

Prepared for the U.S. Department of Energy under Contract Number DE-AC03-76SF00098

DISCLAIMER

LBL-38424
LSBL-313
UC-401

II: A STUDY OF ANGLE-RESOLVED PHOTOEMISSION EXTENDED FINE STRUCTURE AS APPLIED TO THE CU 3*s* AND CU 3*p* CORE-LEVELS OF A CLEAN CU(111) SURFACE*

W.R.A. Huff[a,b], Y. Chen[c], S.A. Kellar[a,b], E.J. Moler[a,b], Z. Hussain[a], Y. Zheng[d], and D.A. Shirley[c]

[a]Advanced Light Source, Lawrence Berkeley National Laboratory, University of California, Berkeley, California 94720
[b]The University of California, Department of Chemistry, Berkeley, California 94720
[c]The Pennsylvania State University, Department of Chemistry and Physics, University Park, Pennsylvania 16802
[d]Present address: Oplink, San Jose, California 95131

*This work was supported by the Director, Office of Energy Research, Office of Basic Energy Sciences, Chemical Sciences Division, of the U.S. Department of Energy, under Contract No. DE-AC03-76SF00098.

II: A Study of Angle-Resolved Photoemission Extended Fine Structure as Applied to the Cu 3*s* and Cu 3*p* Core-Levels of a Clean Cu(111) Surface

W.R.A. Huff,[a,b] Y. Chen,[c] S.A. Kellar,[a,b] E.J. Moler,[a,b]
Z. Hussain,[a] Y. Zheng,[d] and D.A. Shirley[c]

[a]Lawrence Berkeley National Laboratory, Berkeley, CA 94720
[b]The University of California, Dept. of Chemistry, Berkeley, CA 94720
[c]The Pennsylvania State University, Dept. of Chemistry and Physics, University Park, PA 16802
[d]Present address: Oplink, San Jose, CA 95131

ABSTRACT

A clean Cu(111) single crystal was used to study angle-resolved photoemission extended fine structure (ARPEFS) from non-*s* initial states in a controlled manner. Photoemission data from the Cu 3*s* core-level and the Cu 3*p* core-levels were similar but 180° out of phase as expected. The Fourier transform of these clean surface ARPEFS data resemble data for adsorbate systems, showing strong backscattering signals from atoms up to four layers below the source atoms. In addition to the backscattering, the Fourier transform of the Cu 3*p* data show a peak corresponding to scattering from the six nearest neighbor atoms in the same crystal layer as the emitting atoms. Evidence was also seen for single-scattering events from atoms laterally distant from the emitting atom as well as double-scattering events. Multiple-scattering modeling calculation results indicate that the Cu 3*p* photoemission intensity has mostly *d*-wave character. Test calculations indicate that Cu 3*s* photoemission scatters from atomic potentials that are laterally distant from the photoemitter. Also, double-scattering events can be observed in the Cu 3*p* Fourier transform. Additional test calculations show that the ARPEFS signal is dominated by photoemission from atoms in the first two crystal layers.

PACS Number: *61.14.-x, 61.14.Qp, 61.14.Rq, 68.35.Bs, 68.55.Jk*

I. INTRODUCTION

Angle-resolved photoemission extended fine-structure (ARPEFS) is a proved technique for determining surface structures.[1-5] ARPEFS has been used to determine the structures of metal and non-metal atomic adsorbate systems as well as molecular adsorbates on conducting single crystal surfaces. ARPEFS yields accurate information about both the local structure around the adsorbates and the adsorbate-induced relaxation of the substrates.[6-12]

In using ARPEFS to study clean surfaces, the photoelectron signals from surface and bulk atoms will in some cases be resolvable, either directly or through fitting procedures. In these cases, the data analysis would be based on two ARPEFS curves. For the more common case in which signals from different layers cannot be resolved, reconstruction or relaxation effects may still be modeled by fitting the single experimental ARPEFS curve.

Most of the previous ARPEFS studies have been based on photoemission data from atomic s core-level initial states, for which the selection rules $\Delta\ell_i = \pm 1$, and $\Delta m_i = 0$ give a p_o-wave final state. Experience with ARPEFS data from non-s initial states and their Fourier transforms is very limited, however.[13-16] For non-s initial states ($\ell_i \neq 0$), partial waves with orbital quantum numbers $\ell_i + 1$ and $\ell_i - 1$ make up the photoemission intensity. There is a phase relationship between them which leads to interference between the partial waves. Note that the allowed m levels will be populated in the final state. Thus, with a p initial state, the partial waves consist of $\ell_f = 0$, $m_f = m_i = 0$ as well as $\ell_f = 2$, $m_f = m_i = 0, \pm 1$. It is important to note that the intensities sum from these different m levels, not the amplitudes.[17] The intensities also sum over the

different emitters, e. Thus, for the given partial waves, $\psi_{\ell_f,m}(\theta,\phi,k)$, the total intensity, $I_{tot}(\theta,\phi,k)$, is

$$I_{tot}(\theta,\phi,k)=\sum_{e}\sum_{m}\left|\sum_{\ell_f}(-i)^{\ell_f}R_{\ell_f}(k)e^{i\delta_{\ell_f}(k)}\left\langle Y_{\ell_f,m}\left|Y_{1,0}\right|Y_{\ell_i,m}\right\rangle\psi_{\ell_f,m}(\theta,\phi,k)\right|^2 \quad (1)$$

$\left\langle Y_{\ell_f,m}\left|Y_{1,0}\right|Y_{\ell_i,m}\right\rangle$ is the overlap integral between the initial and final spherical harmonic wave functions which are functions of θ and ϕ. $R_{\ell_f}(k)$ are the partial wave radial dipole matrix elements and $\delta_{\ell_f}(k)$ are the phase shifts. Despite these complications, there are a number of interesting experimental situations for which ARPEFS studies on a non-*s* initial state may be the only practical method of study.

A clean Cu(111) single crystal was used to study ARPEFS from non-*s* initial states in a controlled manner. Photoemission data were taken from the Cu 3*p* core-levels and subsequently the Cu 3*s* core-level. The two data sets were acquired on the same sample within a few hours of each other. This allows for a direct comparison of the data and the Fourier transforms.

After fitting the data to determine the parameters, two types of test calculations were performed. For the purpose of determining if double-scattering may be detectable directly in the Fourier transform (FT), a cluster was used with a single emitter adsorbed on a layer of scattering potentials. The single-scattering calculation results are compared to the double-scattering calculation results for each initial state. A second test system used a ten layer cluster for full multiple-scattering calculations. A single emitter was placed in the surface layer; the position of this emitter was subsequently moved to each layer ending with the sixth. The intensity as a function of the magnitude of the photoelectron wave vector is plotted to better understand

from where the ARPEFS signal originates. Each of these test systems is useful to study the similarities and differences between photoemission from the two different initial states.

II. EXPERIMENTAL

The experiments were performed using the Advanced Light Source at the E. O. Lawrence Berkeley National Laboratory on beamline 9.3.2. This is a soft x-ray spherical grating monochromator.[18] The accessible photon energy range was 200 - 800 eV using the 600 $^{lines}/_{mm}$ grating. Because this is not a high-resolution study, the entrance slit was set to 1 mm and the exit slit was set to 120 μm to allow the maximum flux with adequate resolution.

The data were collected in an ultra-high vacuum chamber ($P \leq 60$ nPa) which has been described previously.[16,19] The crystal was spotwelded to a molybdenum sample holder using tantalum strips onto a high-precision manipulator (x, y, z, θ, ϕ) equipped with a liquid-helium cooled cryostat. The crystal was cleaned by repetitive cycles of Ar^+ sputtering and subsequent annealing by electron bombardment from behind to 700 °C. The sample cleanliness was monitored using x-ray photoelectron spectroscopy (XPS) and checking for carbon (1s), nitrogen (1s), oxygen (1s), and sulfur (2p). The Cu 3p data were collected first; the data collection time was five hours for each set. Between the data sets, the sample was annealed to a dim orange glow to desorb any contaminants. The crystal was cooled to ~80 K throughout the data collection.

The photoemission spectra were collected using an angle-resolving electrostatic hemispherical electron energy analyzer (mean radius of 50 mm) which is rotatable 360° around the sample's vertical axis and 100° around the

sample's horizontal axis. The analyzer pass energy was set to 32 eV. The angular resolution of the double einzel input lens was ~±3°.

The degree of linear polarization was measured to be ≥0.99 at the endstation of this bending magnet beamline.[18] The angle of incidence of the light on the crystal was oriented 80° from the surface normal. The photon polarization vector, $\vec{\varepsilon}$, was thus oriented 10° from the surface normal (see illustration in figure 2). The analyzer was oriented 5° off-normal from the Cu(111) surface.

III. DATA COLLECTION

The raw data are a series of photoemission spectra. The photoelectron kinetic energy for the respective Cu 3*s* and Cu 3*p* peaks was stepped from ~100 - 540 eV. Using the de Broglie relation

$$k\left(\text{Å}^{-1}\right) = 0.5123\sqrt{E(\text{eV})} \qquad (2)$$

this photoelectron energy range corresponds to the magnitude of the photoelectron wave vector range ~5.0 - 11.9 Å^{-1}. The spectra were recorded across this range in equal 0.10 Å^{-1} steps.

Each Cu 3*s* photoemission spectrum was a 13 eV window as illustrated in figure 1a. Each Cu 3*p* photoemission spectrum was a 20 eV window encompassing the Cu $3p_{3/2}$ and Cu $3p_{1/2}$ peaks as illustrated in figure 1b. The data reduction for these Cu spectra was much easier than for clean Ni photoemission spectra.[16] The two satellites present in the clean Ni data are not present in either of the clean copper data sets. Also, due to the lack of satellites and thus a lower uncertainty in the determined peak area, it is

expected that the resultant ARPEFS $\chi(k)$ curve represents a more accurate diffraction pattern.

The fits used to determine the peak areas are also included in figures 1a and 1b. Each peak was fit with a Lorentzian convoluted with a Gaussian, a Voigt function, to model the natural linewidth and the experimental broadening, respectively. Each Voigt function was added to a Fermi step-function with a step-height scaled to the respective peak intensity and a step-width taken as the Gaussian width of the respective peak. In this way, the step-function models the inelastic scattering background of the photoemission spectrum. Summing these sub-spectra gives the total fit which is the solid line through the data points. Note that two ARPEFS $\chi(k)$ curves were determined for the Cu $3p$ spectra due to the spin-orbit splitting. As was expected, these two curves were nearly identical. Thus, the reported Cu $3p$ $\chi(k)$ curve is the average of the Cu $3p_{3/2}$ and the Cu $3p_{1/2}$ $\chi(k)$ curves.

IV. DATA REDUCTION AND ANALYSIS

After the peak area is determined from fitting the raw spectra, the data are reduced to the $\chi(k)$ diffraction curve which contains the structural information. $\chi(k)$ is defined by[20]

$$\chi(k) = \frac{I(k)}{I_0(k)} - 1 \qquad (3)$$

where $I(k)$ is the peak area plotted as a function of the peak position in k-space. $I_0(k)$ is a smooth, slowly varying function with an oscillation frequency much lower than $I(k)$; $I_0(k)$ stems from the contribution of the

inelastic scattering processes and the varying atomic cross section. It is adequate to use a simple polynomial function of energy to fit $I_0(k)$.[21]

Removing $I_0(k)$ results in a removal from the Fourier transform the peaks $\lesssim 2$ Å. Note that this study is of the clean copper surface and thus photoemission occurred from atoms several layers below the surface. Many forward scattering path-length differences from sub-surface emitting atoms will be on the order of $\lesssim 2$ Å. The forward scattering signal is therefore removed during the data reduction along with the standard $I_0(k)$. The resulting experimental ARPEFS $\chi(k)$ curve is thus dominated by backscattering.

Figure 2 overlays the Cu 3*s* and the Cu 3*p* ARPEFS $\chi(k)$ curves. The experimental geometry is also pictured. The data are plotted in this way to clearly illustrate that the ARPEFS data from an *s* atomic core-level are ~180° out of phase from ARPEFS data from a *p* atomic core-level. This result is expected and has been studied previously.[13-16]

A. Fourier Analysis

The auto-regressive linear prediction based FT (ARLP-FT) transforms the data from momentum space to real space. In ARPEFS, the positions of the strong peaks in ARLP-FTs from adsorbate/substrate systems can be predicted with fairly good accuracy using the single-scattering cluster model together with the concept of strong backscattering from atoms located within a cone around 180° from the emission direction.

These FT peaks correspond to path-length differences (PLDs) between the component of the photoemitted wave that propagates directly to the detector and the components which are first scattered by the atomic

potentials within this backscattering cone.[6] The scattering takes place inside the crystal and the ARPEFS data must be shifted from the measured $\chi\left(k_{\text{outside-crystal}}\right)$ to $\chi\left(k_{\text{inside-crystal}}\right)$ to account for the inner potential. In ARPEFS modeling calculations, the inner potential is often treated as an adjustable parameter and is typically 5 - 15 eV. The inner potential is approximately the sum of the work function and the valence band-width.[22] The work function for Cu(111) is ~5 eV and the valence band-width is ~5 eV.[23,24] Thus, before Fourier transformation, the ARPEFS data presented here were shifted by 10 eV to higher kinetic energy.

Figure 3 plots the ARLP-FT of the Cu 3*s* and the Cu 3*p* ARPEFS data. Also illustrated in figure 3 is a schematic of the Cu(111) single crystal, assuming a bulk-terminated fcc surface, with a backscattering cone superimposed. The FT shows peaks due to scattering from atoms up to four layers below the emitting atoms. The depth sensitivity of ARPEFS has been described previously and was found to be enhanced by multiple-scattering effects.[5]

The labeled atoms correspond to the labeled peaks in figure 3. Using the bulk nearest-neighbor spacing, 2.56 Å, and assuming a bulk-terminated surface, the expected peak positions can be calculated using simple geometry. These expected peak positions are listed in table 1 along with the actual peak positions (and corresponding shifts) for the Cu 3*s* and Cu 3*p* data FTs. Also listed in table 1 is an assignment of the peak to single-scattering (SS) or double-scattering (DS) events. Additionally, the number of atomic scattering potentials contributing to each peak is listed in table 1.

The origins of the peaks labeled 2, 3, 4, 5, and 6 are straightforward. If a line is drawn from a surface emitter into the crystal and normal to the (111) plane, peaks 2, 3, and 6 occur due to single-scattering from the three

atoms closest to this line in layers 2, 3, and 5, respectively. Copper is fcc and thus peak 4 is due to direct backscattering (θ_j=180°) from the #4 atom which is in layer 4. Peak 5 is due to single-scattering from the six nearest neighbors to atom #4, the #5 atoms which are also in layer 4.

Peaks 2' and 3' may be attributed to atoms more laterally distant from the line described above. Peak 2' occurs due to single-scattering from the three second nearest-neighbors to this line in layer 2. Similarly, peak 3' occurs due to single-scattering from the three second nearest-neighbors to this line in layer 3.

Double-scattering may be detectable in the ARLP-FT as evidenced by peaks 2*, 3*, 4*, and 5*. The first event for peak 2*, for example, is scattering by the three #2 atoms. The second event is scattering by the six nearest-neighbors to each #2 atom. An analogous process holds for the 3* peak. Because there is only one #4 atom for each emitter in the fcc ($\dot{a}bc\dot{a}bc$) geometry, only six atoms are in position for the second scattering event to give peak 4*. However, there are six #5 atoms and thus thirty-six atoms for the second scattering event to give peak 5*.

An additional peak is noted in the Cu 3*p* ARLP-FT. The peak labeled 1 is due to single-scattering of the photoemitted wave from the six nearest neighbor atoms in the same (111) plane as the emitting atoms. This scattering path is not observed in the Cu 3*s* FT and has not been observed previously for *s* initial state data or calculations. The photoemitted p_0-wave final state destructively interferes with itself for the scattering angle $\theta_j = 90°$ due to its negative parity. From the *p* initial state, however, the photoemitted *d* and *s* partial waves which are interfering with themselves and with each other have positive parity. Therefore, they do not cancel upon scattering from atoms in the same (111) plane as the emitting atoms. This result has

been seen previously for ARPEFS data collected from the Ni 3*p* core-level of clean Ni(111).[16]

An interesting feature of the Cu 3*s* FT as compared to the Cu 3*p* FT is the intensity differences between some of the peaks. If the ARPEFS data from these different initial states were identical but out of phase, then their FTs would be identical in peak position and intensity. These data are more than simply out of phase as evidenced by the appearance of peak 1 in the Cu 3*p* FT which is not present in the Cu 3*s* FT. A related study of ARPEFS data collected from the sulfur 1*s* and 2*p* initial states for c(2x2)S/Ni(001) found that the generalized Ramsauer-Townsend effect[25] occurs in the S 1*s* data but not the S 2*p* data.[13]

The total photoemitted intensity, $I_{\text{tot}}(\theta,\phi,k)$, was discussed in the introduction. Given that $I_{\text{tot}}(\theta,\phi,k)$ depends on the initial state, the oscillation magnitudes in the respective $\chi(k)$ curves should be somewhat different. These differences translate to the FT as intensity differences between the two initial state ARPEFS data for a given PLD.

From the single-scattering values listed in table 1, one can see that the structure can generally be determined to ±0.5 Å by simply analyzing the ARLP-FT. Given this accuracy limit, some peaks seem to correlate with double-scattering PLDs. However, these assignments due to double-scattering events are somewhat speculative. To be certain that these small features are not artifacts caused by the finite data range, one must study the FT in more detail than has been done to date. Additionally, one must better understand any slight shifting of the peaks caused by mathematically extending the data range using the ARLP method.

B. Multiple Scattering Analysis

It has become standard to perform modeling calculations in an attempt to simulate ARPEFS $\chi(k)$ curves. Using the single-scattering model of ARPEFS,[6,20] $\chi(k)$ can be written as

$$\chi(k) = \sum_j A_j(k) \cos\left[k\left(R_j - R_j \cos\theta_j\right) + \phi_j\right] \tag{4}$$

where $A_j(k)$ contains experimental geometry factors including the photon polarization direction and the electron emission direction as well as the scattering amplitude, aperture integration, and thermal averaging.

A new code developed by Chen, Wu, and Shirley was used for the calculations presented here.[17,26-28] Fitting calculations can be performed for systems in which the photoemitters are in many layers and the core-level initial state has arbitrary angular momentum. For fitting the Cu 3*p* initial state data, the radial dipole matrix elements, $R_{\ell_i \pm 1}$, and phase shifts, $\delta_{\ell_i \pm 1}$, were obtained from Goldberg, Fadley, and Kono[29] who developed them from Manson and Cooper's earlier work.[30] These values describe the shape and phase relationship between the photoemitted partial waves, $\ell_i \pm 1$.

To account for vibration effects of the bulk atoms, the mean square relative displacement was calculated using equation (33) by Sagurton *et al.*[4] The correlated Debye temperature was 350 K and the sample temperature was 80 K for both data sets. Accounting for the surface atomic vibration has been discussed previously.[12,31]

The inelastic mean free path was included using the exponential damping factor $e^{-r/\lambda}$ where λ was calculated using the Tanuma, Powell, and Penn (TPP-2) formula.[32] The analyzer acceptance angle was set to match the

experiment as described earlier. The atomic-scattering phase shifts were calculated in situ by using the atomic potentials tabulated by Moruzzi *et al.*[33] The emission direction was optimized at 5° off-normal and the polarization direction was optimized at 180°, the [111] direction. Optimization of the emission and polarization angles is discussed in the next section.

Figure 4a overlays the experimental Cu 3*s* ARPEFS data (solid line) with its best fit (dashed line). Figure 4b overlays the experimental Cu 3*p* ARPEFS data (solid line) with its best fit (dashed line). For each fit, a 74 atom cluster was used. During the fitting, the distance between the first two copper layers, $d_{1,2}$,was unusually sensitive to the inner potential.[12,16] This resulted in a large uncertainty in the determined structure. Thus, the inner potential was fixed at 10 eV as discussed above. The modeling calculations determined that $d_{1,2}$ = 2.06(5) Å, a contraction from the bulk value, 2.09 Å. This surface layer contraction is consistent with previous LEED studies which found a contraction of 0.7(5) %.[34,35] By contrast, there is a slight surface *expansion* (+1.5%) of the clean Ni(111) surface; $d_{1,2}$ = 2.06(1) Å while the bulk Ni(111) spacing is 2.03 Å.[16]

C. Discussion of Error

Since the purpose of this work is to study final-state effects in ARPEFS, it is useful to minimize the *R*-factor as a function of the emission angle as measured from the surface normal, θ_e, and the azimuthal angle about the surface normal, ϕ_e. These contour plots are illustrated in figures 5a and 5b for the Cu 3*s* and Cu 3*p* fitting calculations, respectively. The sample's orientation with respect to the photon beam, and thus the photon polarization vector, was maintained constant. θ_e was varied from 0° to +10°

stepping by 1° and ϕ_e was varied from 0° to 180° stepping by 10°. The fcc surface has six-fold symmetry but the bulk only has three-fold symmetry; the surface atoms adsorb in the three-fold hollow site. $\phi_e = 0°$ was chosen to bisect one edge of the equilateral triangle formed by this three-fold hollow site, the [100] direction. Thus, a mirror plane exists which allows the calculations to be symmetrized to obtain the results for $\phi_e = 180°$ to 360°.

Comparing figures 5a and 5b shows some very interesting differences between the Cu 3*s* and the Cu 3*p* ARPEFS data. From figure 5a (the Cu 3*s* contour plot), the *R*-factor minimum is at $\theta_e = 4.5° \pm 1°$. It is a very shallow minimum toward normal emission ($\theta_e = 0°$) but becomes steep more off-normal ($\theta_e > 5°$). When visually inspecting the Cu 3*s* fits, $\theta_e = 5°$ fit was marginally better than the $\theta_e = 0°$. Figure 5b (the Cu 3*p* contour plot) is markedly different due to final-state effects. The *R*-factor minimum is at $\theta_e = 5.5° \pm 0.5°$. It is a very steep minimum both toward and away from normal emission ($\theta_e < 5°, \theta_e > 6°$). For the Cu 3*p*, the $\theta_e = 0°$ fit was very poor while the $\theta_e = 5°$ fit was quite good. This result has significant implications with respect to modeling ARPEFS data from non-*s* initial states. As always, great care must be taken during the alignment of the experimental system. Additionally, because the difference of 1° is so important, the modeling must search angle-space to finally obtain the optimum fit to the data.

Studying how the *R*-factor varies with ϕ_e at different θ_e also shows final-state effects. For both the 3*s* and the 3*p* initial states, the *R*-factor is very insensitive to changing ϕ_e if θ_e is near normal emission ($\theta_e < 5°$). Even at the *R*-factor minimum ($\theta_e \approx 5°$), the *R*-factor remains rather insensitive to changing ϕ_e. However, for the 3*p* initial state, the three-fold symmetry of the adsorption site begins to become evident. As θ_e is increased even more ($\theta_e > 5°$), the *R*-factor begins to vary significantly with changing ϕ_e and the

three-fold symmetry of the adsorption site is evident in both contour plots. This results due to backscattering. As the emission angle becomes more off-normal, backscattering from the second-layer Cu atoms is enhanced in the ARPEFS $\chi(k)$ curve.

As stated above, $\phi_e = 0°$ is toward the [100] direction. This geometry would highlight backscattering from the second-layer Cu atom. Since the best fit to the data is for $\phi_e = 180°$ (as well as +120° and -120° from 180°) it can be concluded that during the experiment, the analyzer was ~5° off-normal toward the [111] direction (away from an edge and toward a point of the equilateral triangle formed by the three-fold hollow adsorption site).

These results from θ_e and ϕ_e indicate that the detected intensity distribution of Cu 3*s* photoemission is less directional than the detected intensity distribution of Cu 3*p* photoemission. As discussed previously, photoemission data from atomic *s* core-level initial states gives a p_o-wave final state. Thus, the intensity distribution from the Cu 3*p* core-level initial states must have mostly *d*-wave character. This is not necessarily intuitive because examining the radial dipole matrix elements shows that R_{ℓ_i+1} (*d* partial-wave) is less than a factor of two greater than R_{ℓ_i-1} (*s* partial-wave) through almost the entire ARPEFS data range.[13,29]

It should be noted that the calculations can be symmetrized as described above because the photon polarization vector is approximately normal to the surface. Experience with fitting ARPEFS data suggests that the oscillation frequencies of the $\chi(k)$ curve are rather insensitive to the photon polarization vector orientation. However, the oscillation amplitudes are dependent on this orientation. These amplitude variations will change the magnitude of the *R*-factor and perhaps break this three-fold symmetry.

Thus, if the photon polarization vector is significantly off-normal, then ϕ_e should be calculated from 0° to 360°.

V. DISCUSSION

A. Double Scattering Events

Using the best-fit parameters, some test calculations were completed to study the scattering in more detail. To determine whether double-scattering events can be detected in the ARLP-FT, a test cluster was input with a single emitter adsorbed 2.06 Å above a layer of scattering atomic potentials. The distance and geometry were chosen such that the layer simulated the second layer of the fcc Cu(111). In addition to testing for double-scattering, this test allows for the simulation of the intensity differences between the Cu 3*s* and Cu 3*p* FTs in figure 3. Note that the ARLP method was not applied to these test $\chi(k)$ curves because they were calculated directly over a wide *k*-range (4 - 20 $Å^{-1}$).

With this geometry, peaks are expected to be at PLDs correlating with the 2 and 2' positions for single-scattering and the 2, 2', and 2* positions for double-scattering. Figure 6a plots the Cu 3*s* FT for a single-scattering calculation (solid line) and a double-scattering calculation (dashed line). Figure 6b plots the Cu 3*p* FT for a single-scattering calculation (solid line) and a double-scattering calculation (dashed line). The respective $\chi(k)$ curves are plotted in the insets. The $\chi(k)$ curves were filtered to pass only those PLDs > 3.5 Å to remove some low frequency oscillations unrelated to PDLs. The 2* peak distinctly appears in the FT of the Cu 3*p* double-

scattering calculation even though there appear to be only minor differences in the $\chi(k)$ curves. The 2* peak is not as convincing in the Cu 3*s* FT.

A striking difference between the Cu 3*s* and Cu 3*p* FTs is the occurrence of peaks 2" and 2"' in only the Cu 3*s* FT. Each additional prime represents scattering from the next laterally distant atomic potential. This difference is also observed in the ARLP-FT of the ARPEFS data for the peak $\lesssim$7 Å and is the reason for the chosen 2* position in figure 3. These results again indicate that Cu 3*p* photoemission intensity is more directional than the Cu 3*s* photoemission intensity.

B. Contribution of Emitters in Different Layers

For the study of clean surfaces or multilayers, it is important to understand the contribution of emitters in sub-surface layers to the overall ARPEFS data. For these tests, a ten layer fcc Cu(111) cluster was input with a single emitter. This emitter was subsequently moved from the surface to each layer, ending with the sixth. The cluster was constructed such that the photoemitted wave from the emitter in the sixth layer was subject to the same scattering environment as the photoemitted wave from the emitter in the surface layer. This is true to four layers below the emitter which is the cut-off seen in the ARLP-FT of the ARPEFS data.

Figure 7 shows the multiple-scattering calculation results for this test cluster. The calculation parameters were fixed at the best-fit values discussed previously. The normalized intensity at the detector is plotted as a function of the magnitude of the photoelectron wave vector. The first point to note about these results is that the signal from the Cu 3*s* initial state is a factor of 100 stronger than the signal from the Cu 3*p* initial state. This factor

drops out in equation (2) and is thus not seen in the data $\chi(k)$ curves. The next point to note is that the signal drops off drastically between placing the emitter in the second layer and placing the emitter in the third layer. The signal increases slightly when placing the emitter in the fourth layer due to forward focusing by the surface layer atoms.

When the emitter is placed from the third layer to the sixth layer, the high-frequency oscillations important to ARPEFS become small and the $I(k)$ curves become dominated by the low-frequency oscillations (short path-length differences). This indicates that the signal is becoming dominated by forward scattering.

The bottom panel in figure 7 plots $I_{\text{total}}(k)$ which is the sum of the six calculated $I(k)$ curves. This curve simulates the total intensity that would be collected. The low-frequency oscillations are removed by equation (2) when $I(k)$ is divided by a simple polynomial to fit $I_0(k)$. The forward scattering signal is therefore removed during the data reduction along with the standard $I_0(k)$. The resulting experimental ARPEFS $\chi(k)$ curve is thus dominated by backscattering. Although the signal from the deeper layers may modulate the high-frequency oscillation magnitudes slightly, the signal is principally due to photoemission from the first two crystal layers. Scattering from six or seven layers is therefore adequate to simulate ARPEFS data.

VI. CONCLUSION

A Cu(111) single crystal sample was used to study ARPEFS from non-*s* initial states in a controlled manner. Photoemission data were taken from the Cu 3*p* core-levels and subsequently the Cu 3*s* core-level. These

two data sets were similar but ~180° out of phase as expected. The Fourier transform of these clean surface ARPEFS data resemble data for adsorbate systems, showing strong backscattering signals from atoms up to four layers *below* the source atoms. In addition to the backscattering, the FT of the Cu $3p$ data show a peak corresponding to scattering from the six nearest neighbor atoms in the same crystal layer as the emitting atoms. This result is forbidden by symmetry for s initial state photoemission scattering from a point source but is expected from p initial state photoemission. Evidence was also seen for single-scattering events from atoms laterally distant from the emitting atom as well as double-scattering events.

The R-factor was minimized as a function of ϕ_e and θ_e. These contour plots illustrate the directional nature of the Cu $3s$ as compared to the Cu $3p$ photoemission intensity distribution. For the Cu $3s$ fitting, the R-factor minimum is rather shallow from $0° < \theta_e < 5°$. However, at $\theta_e > 5°$, the Cu $3s$ R-factor rises sharply and changing ϕ_e begins to show the three-fold symmetry of the adsorption site. In contrast, the Cu $3p$ R-factor minimum is very steep for $\theta_e < 5°$ and $\theta_e > 6°$. The three-fold symmetry in ϕ_e is not evident until $\theta_e \geq 5°$. These results indicate that the photoemission intensity from the Cu $3p$ core-levels must have mostly d-wave character. Because $\Delta\theta_e = 1°$ has such a dramatic effect on the quality of the fit, the modeling must search angle-space to obtain the optimum fit to the data.

After fitting the data to determine the parameters, two types of test calculations were performed. For the purpose of determining if double-scattering events may be detectable directly in the FT, a cluster was used with a single emitter adsorbed on a layer of scattering potentials. The 2* peak distinctly appears in the FT of the Cu $3p$ double-scattering calculation even though there appear to be only minor differences in the $\chi(k)$ curves.

The 2* peak is not as convincing in the Cu 3*s* FT. The Cu 3*s* FT, however, indicates scattering from atomic potentials much more laterally distant than the Cu 3*p* FT. These results again indicate that Cu 3*p* photoemission intensity is more directional than the Cu 3*s* photoemission intensity.

A second test system used a ten layer cluster for full multiple-scattering calculations. A single emitter was placed in the surface layer; the position of this emitter was subsequently moved to each layer ending with the sixth. The $I(k)$ curves illustrate that the signal from the Cu 3*s* initial state is a factor of 100 stronger than the signal from the Cu 3*p* initial state. The signal drops off drastically when the emitter is placed below the second layer. From the third layer to the sixth layer, the high-frequency oscillations important to ARPEFS become small and the $I(k)$ curves become dominated by the low-frequency oscillations. Although the signal from the deeper layers may modulate the high-frequency oscillation magnitudes slightly, the photoemission signal comes principally from the first two crystal layers. Scattering from six or seven layers is therefore adequate to simulate ARPEFS data.

ACKNOWLEDGMENTS

These experiments were carried out with the assistance of the personnel at the Advanced Light Source at the E. O. Lawrence Berkeley National Laboratory. This work was supported by the Director, Office of Energy Research, Office of Basic Energy Sciences, Chemical Sciences Division of the U.S. Department of Energy under Contract No. DE-AC03-76SF00098.

TABLES

- Table 1: Scattering paths with the calculated PLD (based on 2.56 Å nearest neighbor spacing) along with the actual peak positions and the respective shifts. Refer to figure 3 for an illustration of the atomic positions.

Peak Number	Calculated PLD (Å)	Cu 3*s* Position (Å)	Cu 3*p* Position (Å)	Scattering Process	# of Atomic Potentials
1	2.56	---	2.39 (-0.17)	SS	6
2	4.65	4.15 (-0.50)	4.85 (+0.20)	SS	3
2'	5.71	6.19 (+0.48)	6.26 (+0.55)	SS	3
2*	7.21	7.67 (+0.46)	7.58 (+0.37)	DS	3 × 6
3	8.61	8.36 (-0.25)	8.29 (-0.32)	SS	3
3'	9.30	8.91 (-0.39)	9.37 (+0.07)	SS	3
3*	11.17	10.91 (-0.26)	10.97 (-0.20)	DS	3 × 6
4	12.54	12.10 (-0.44)	12.46 (-0.08)	SS	1
5	13.04	13.20 (+0.16)	13.12 (+0.08)	SS	6
4*	15.10	14.96 (-0.14)	15.13 (+0.03)	DS	1 × 6
5*	15.60	15.77 (+0.17)	15.80 (+0.20)	DS	6 × 6
6	16.85	16.68 (-0.17)	16.99 (+0.14)	SS	3

FIGURES

- Figure 1: Example photoemission spectrum showing the data as well as the Voigt function(s) and the step function used to fit the a) Cu 3*s* data and b) the Cu 3*p* data.

- Figure 2: Cu(111) 3*s* ARPEFS $\chi(k)$ data (solid line) and Cu(111) 3*p* ARPEFS $\chi(k)$ data (dashed line). A schematic of the experimental geometry is shown.

- Figure 3: ARLP based FTs of the Cu 3*s* data (solid line) and Cu 3*p* data (dashed line). A model of the lattice with the backscattering cone indicates the scattering atoms corresponding to the FT peaks.

- Figure 4: ARPEFS $\chi(k)$ data (solid line) and the MSSW best fit (dashed line) for a) Cu(111) 3*s* and b) Cu(111) 3*p*.

- Figure 5: a) Contour plot showing how the *R*-factor varies with ϕ_e and θ_e for a) the Cu 3*s* modeling and b) the Cu 3*p* modeling.

- Figure 6: FT of the calculated ARPEFS $\chi(k)$ curves (insets) for a) Cu 3*s* and b) Cu 3*p* where a single emitter was adsorbed 2.06 Å above a layer of scattering potentials for single-scattering (solid line) and double-scattering (dashed line).

- Figure 7: The calculated ARPEFS $I(k)$ curves for Cu 3*s* (solid line) and Cu 3*p* (dashed line) where a single emitter was moved successively to deeper layers.

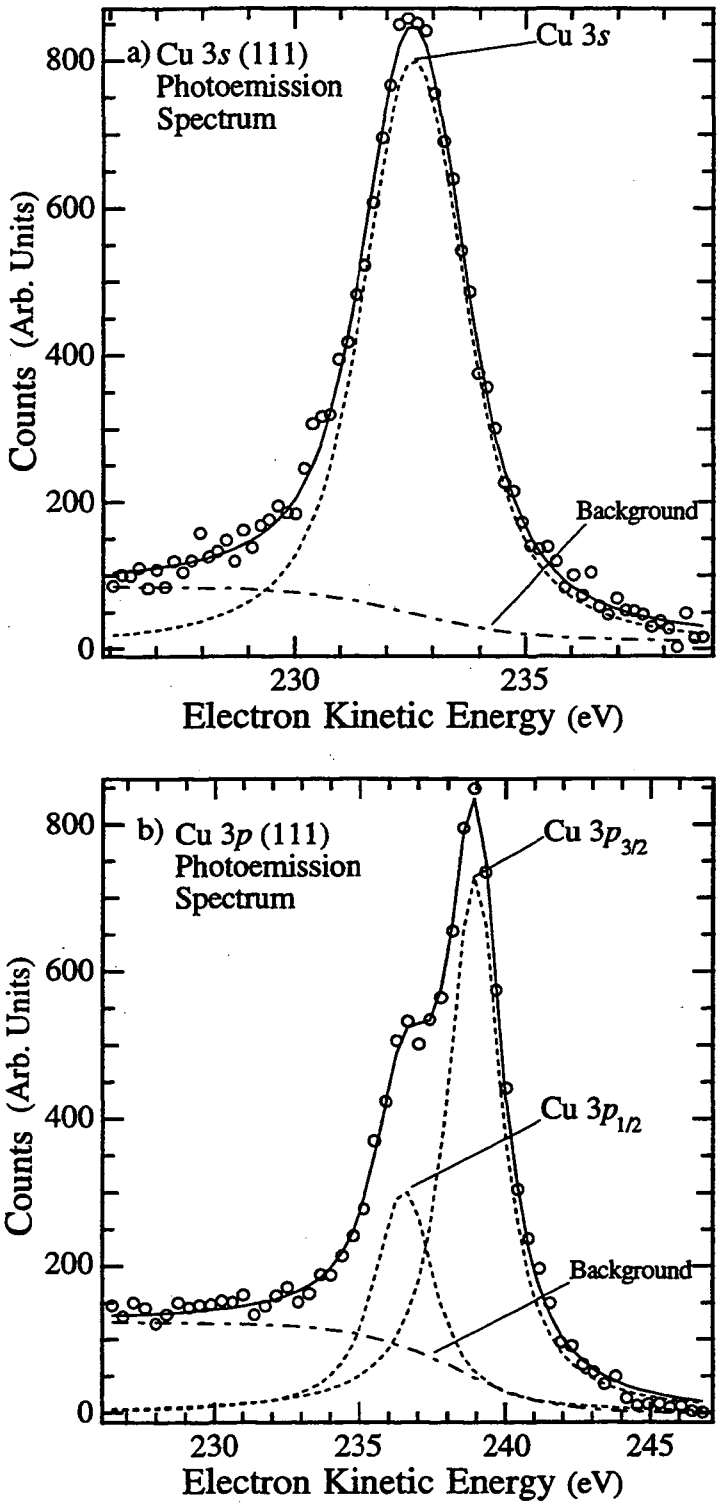

Figures 1a and 1b

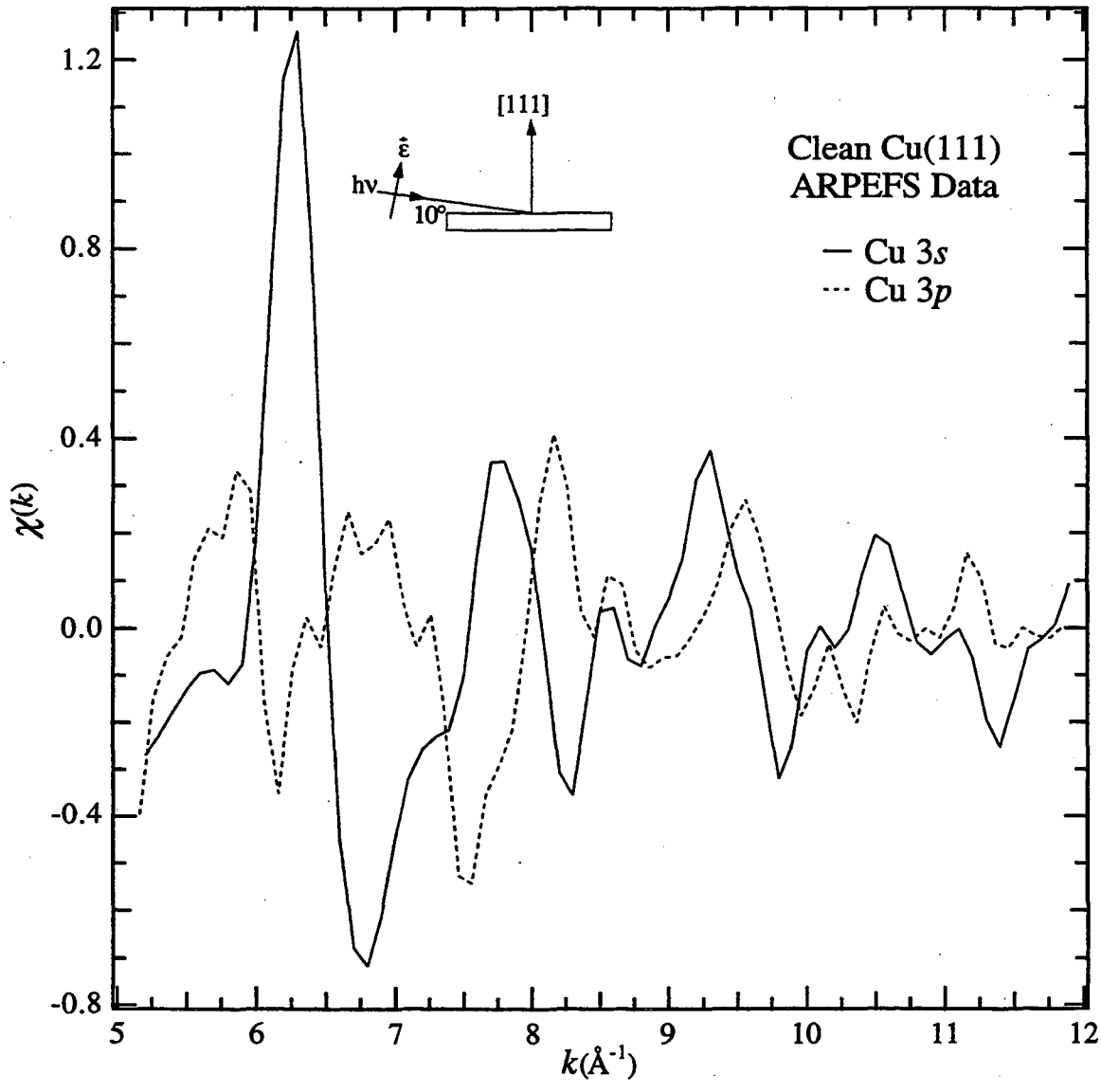
Clean Cu(111)
ARPEFS Data
— Cu 3s
··· Cu 3p
[111]
ε̂
hν
10°
χ(k)
k(Å⁻¹)
1.2
0.8
0.4
0.0
-0.4
-0.8
5
6
7
8
9
10
11
12

Figure 2

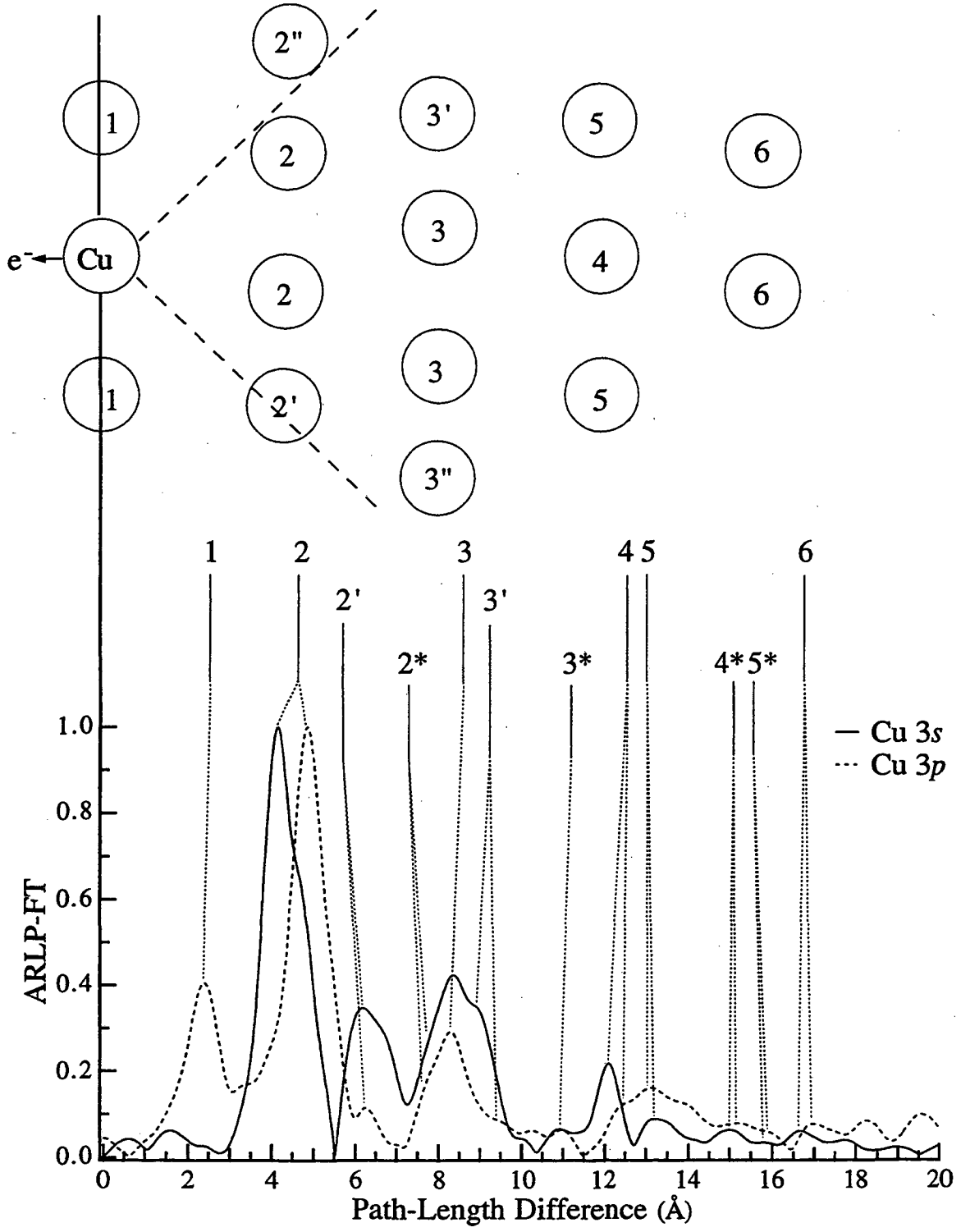
e⁻
Cu
1
2"
2
2
2'
1
3'
3
3
3"
5
4
5
6
6
1
2
2'
2*
3
3'
3*
4*
4 5
5*
6
— Cu 3s
··· Cu 3p
ARLP-FT
0.0
0.2
0.4
0.6
0.8
1.0
0
2
4
6
8
10
12
14
16
18
20
Path-Length Difference (Å)

Figure 3

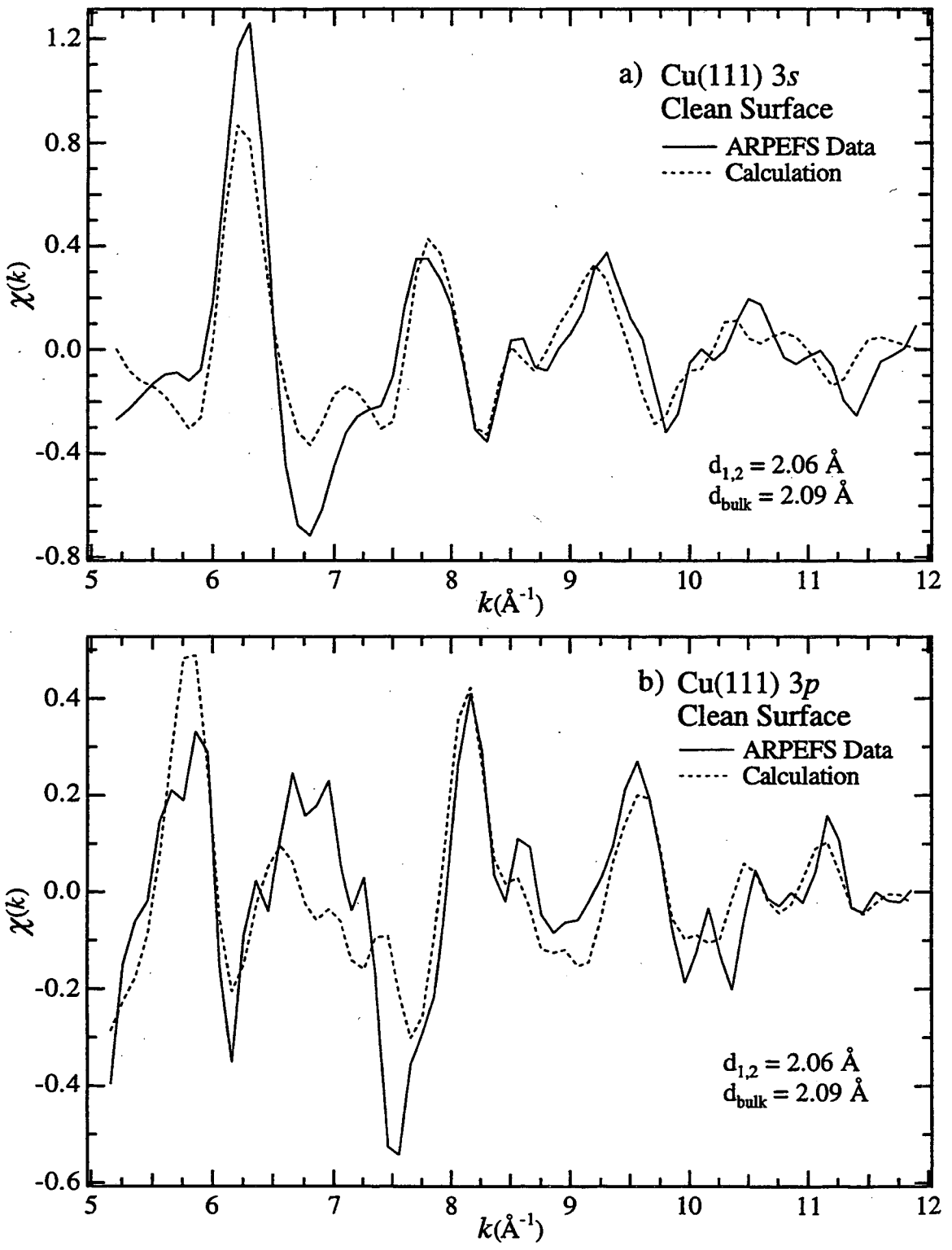

Figures 4a and 4b

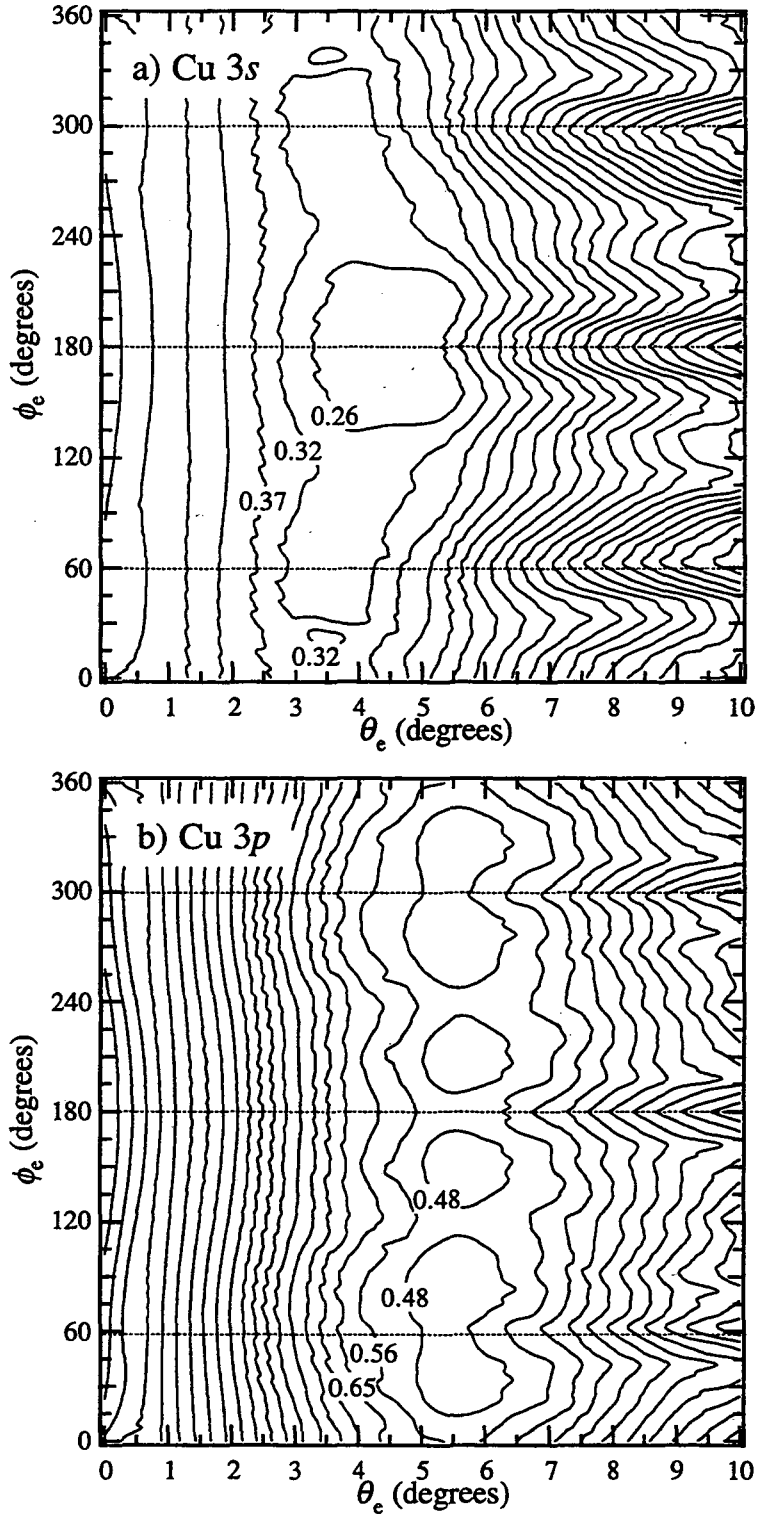

Figures 5a and 5b

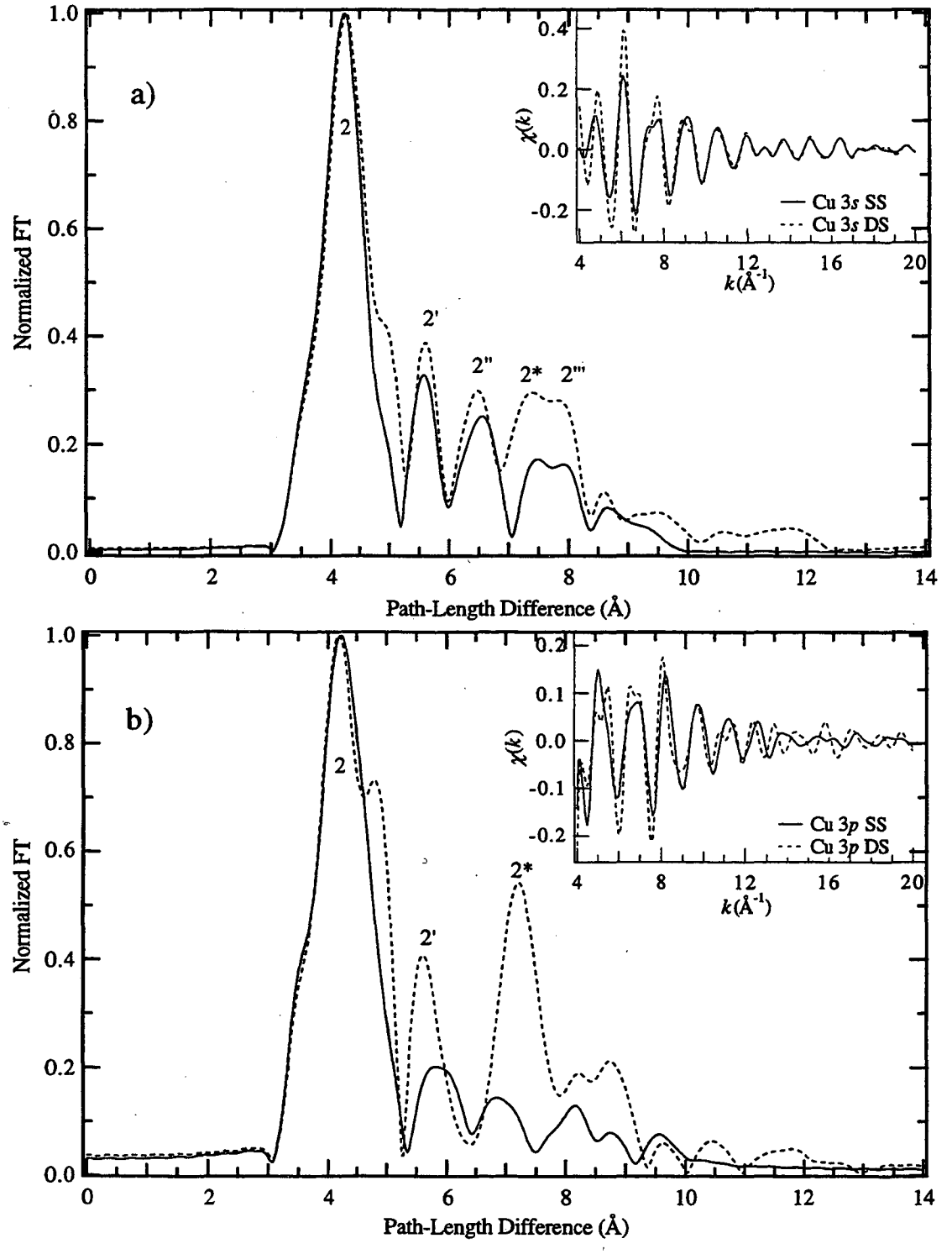

Figures 6a and 6b

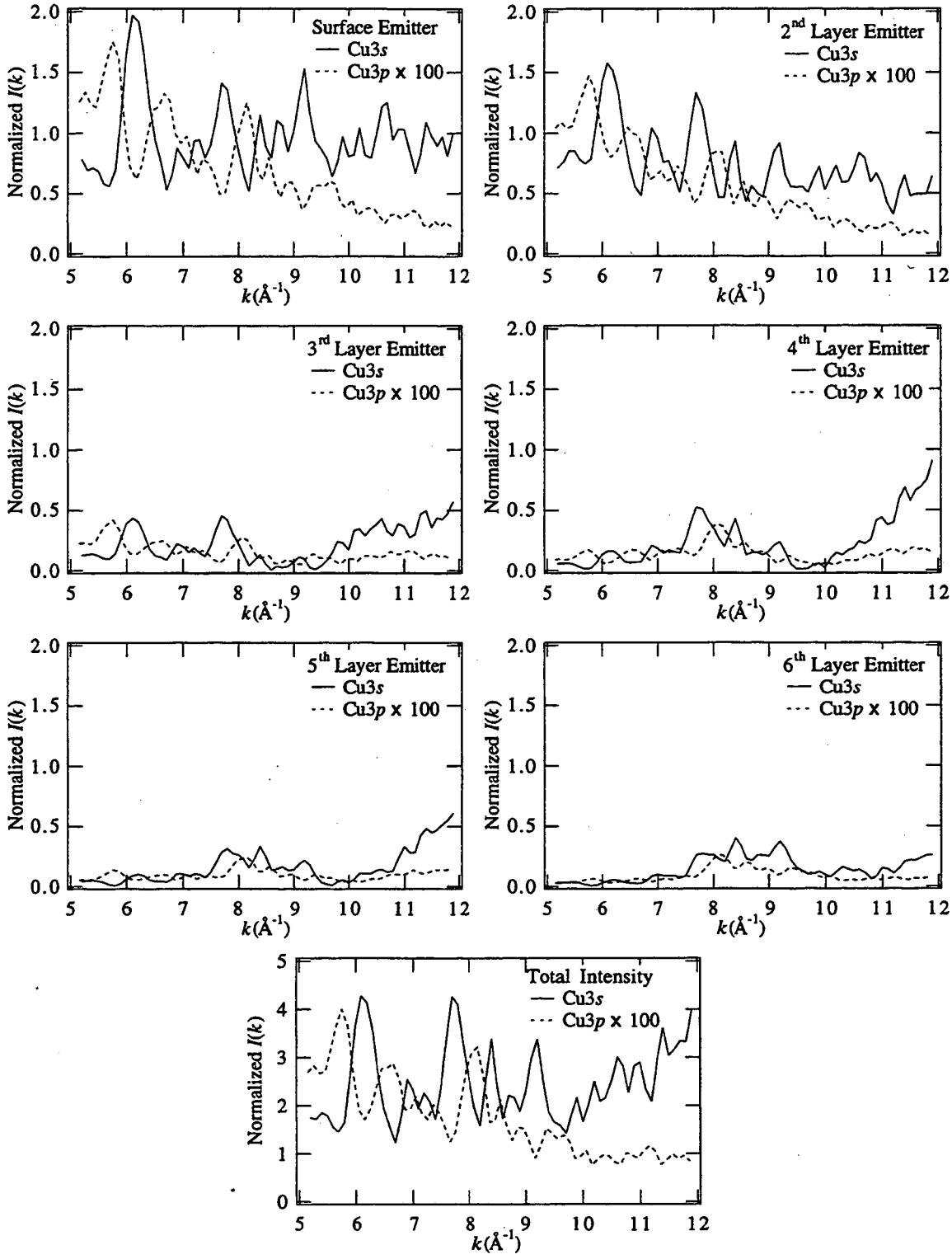
Surface Emitter
Cu3s
Cu3p x 100
2nd Layer Emitter
3rd Layer Emitter
4th Layer Emitter
5th Layer Emitter
6th Layer Emitter
Total Intensity
Normalized I(k)
k(Å-1)

Figure 7

REFERENCES

[1]S.D. Kevan, D.H. Rosenblatt, D. Denley, B.C. Lu and D.A. Shirley, Phys. Rev. Lett. **41**, 1565(1978).

[2]J.J. Barton, C.C. Bahr, Z. Hussain, S.W. Robey, J.G. Tobin, L.E. Klebanoff and D.A. Shirley, Phys. Rev. Lett. **51**, 272(1983).

[3]D.P. Woodruff, D. Norman, B.W. Holland, N.V. Smith, H.H. Farrell and M.M. Traum, Phys. Rev. Lett. **41**, 1130(1978).

[4]M. Sagurton, E.L. Bullock and C.S. Fadley, Surf. Sci. **182**, 287(1987).

[5]Y. Zheng and D.A. Shirley, Chem. Phys. Lett. **203**, 114(1993).

[6]J.J. Barton, C.C. Bahr, S.W. Robey, Z. Hussain, E. Umbach and D.A. Shirley, Phys. Rev. B **34**, 3807(1986).

[7]S.W. Robey, C.C. Bahr, Z. Hussain, J.J. Barton, K.T. Leung, J.R. Lou, A.E. Schach von Wittenau and D.A. Shirley, Phys. Rev. B **35**, 5657(1987).

[8]L.Q. Wang, A.E. Schach von Wittenau, Z.G. Ji, L.S. Wang, Z.Q. Huang and D.A. Shirley, Phys. Rev. B **44**, 1292(1991).

[9]Z.Q. Huang, L.Q. Wang, A.E. Schach von Wittenau, Z. Hussain and D.A. Shirley, Phys. Rev. B **47**, 13626(1993).

[10]Z.Q. Huang, Z. Hussain, W.T. Huff, E.J. Moler and D.A. Shirley, Phys. Rev. B **48**, 1696(1993).

[11]Y. Zheng, E. Moler, E. Hudson, Z. Hussain and D.A. Shirley, Phys. Rev. B **48**, 4960(1993).

[12]W.R.A. Huff, Y. Chen, X.S. Zhang, L.J. Terminello, F.M. Tao, Y.K. Pan, S.A. Kellar, E.J. Moler, Z. Hussain, H. Wu, Y. Zheng, X. Zhou, A.E. Schach von Wittenau, S. Kim, Z.Q. Huang, Z.Z. Yang and D.A. Shirley, (to be published).

[13]W.R.A. Huff, Y. Zheng, Z. Hussain and D.A. Shirley, J. Phys. Chem. **98**, 9182(1994).

[14]S.Y. Tong and J.C. Tang, Phys. Rev. B **25**, 6526(1982).

[15]J.C. Tang, Chin. Phys. Lett. **4**, 321(1987).

[16]W.R.A. Huff, Y. Chen, S.A. Kellar, E.J. Moler, Z. Hussain, Z.Q. Huang, and D.A. Shirley, Part I of this series.

[17]M. Biagini, Phys. Rev. B **48**, 2974(1993).

[18]Z. Hussain, W.R.A. Huff, S.A. Kellar, E.J. Moler, P.A. Heimann, W. McKinney, M.R. Howells, J.B. Kortright, M.A. Rice, C. Cummings, T. Lauritzen, J.P. McKean, S.C. Irick, F.J. Palomares, R.X. Ynzunza, Z. Wang, G. Andronaco, N. Hartman, E.D. Tober, H. Wu, Y. Zheng, A. Adamson, A.T. Young, H. Daimon, H.A. Padmore, C.S. Fadley, D.A. Shirley, (to be published).

[19]S.D. Kevan, *Ph.D. Thesis*, The University of California, Berkeley, LBL-11017(1980).
[20]J.J. Barton, S.W. Robey and D.A. Shirley, Phys. Rev. B **34**, 778(1986).
[21]J.J. Barton, *Ph.D. Thesis*, The University of California, Berkeley, LBL-19215(1985).
[22]L.J. Terminello, *Private Communication*, (1996).
[23]R.C. Weast, *Handbook of Chemistry and Physics*, 67th ed., (CRC Press, Boca Raton, FL, 1986-1987).
[24]P. Thiry, *PhD Thesis*, L'Université Pierre et Marie Curie, Paris, France, (1980).
[25]J.J. Barton, Z. Hussain and D.A. Shirley, Phys. Rev. B **35**, 933(1987).
[26]Y. Chen, H. Wu and D.A. Shirley, *CWMS Code - Unpublished*, (1995).
[27]J.J. Rehr and R.C. Albers, Phys. Rev. B **41**, 8139(1990).
[28]D.J. Friedman and C.S. Fadley, J. Electron Spectrosc. Relat. Phenom. **51**, 689(1990).
[29]S.M. Goldberg, C.S. Fadley and S. Kono, J. Electron Spectrosc. Relat. Phenom. **21**, 285(1981).
[30]S.T. Manson and J.W. Cooper, Phys. Rev. **165**, 126(1968).
[31]R.E. Allen, G.P. Alldredge and F.W. de Wette, J. Chem. Phys. **54**, 2605(1971).
[32]S. Tanuma, C.J. Powell and D.R. Penn, Surf. Interface Anal. **20**, 77(1993).
[33]V.L. Moruzzi, J.F. Janak and A.R. Williams, *Calculated Electronic Properties of Metals*, (Pergamon Press, Inc., New York, 1978).
[34]S.P. Tear, K. Roll and M. Prutton, J. Phys. C **14**, 3297(1981).
[35]S.A. Lindgren, L. Wallden, J. Rundgren and P. Westrin, Phys. Rev. B **29**, 576(1984).

LAWRENCE BERKELEY NATIONAL LABORATORY
UNIVERSITY OF CALIFORNIA
TECHNICAL & ELECTRONIC INFORMATION DEPARTMENT
BERKELEY, CALIFORNIA 94720